

Alma Mater Studiorum Università di Bologna  
Archivio istituzionale della ricerca

Hierarchical electrospun tendon-ligament bioinspired scaffolds induce changes in fibroblasts morphology under static and dynamic conditions

This is the final peer-reviewed author's accepted manuscript (postprint) of the following publication:

*Published Version:*

Sensini A., Cristofolini L., Zucchelli A., Focarete M.L., Gualandi C., de Mori A., et al. (2020). Hierarchical electrospun tendon-ligament bioinspired scaffolds induce changes in fibroblasts morphology under static and dynamic conditions. JOURNAL OF MICROSCOPY, 277(3), 160-169 [10.1111/jmi.12827].

*Availability:*

This version is available at: <https://hdl.handle.net/11585/760027> since: 2021-03-02

*Published:*

DOI: <http://doi.org/10.1111/jmi.12827>

*Terms of use:*

Some rights reserved. The terms and conditions for the reuse of this version of the manuscript are specified in the publishing policy. For all terms of use and more information see the publisher's website.

This item was downloaded from IRIS Università di Bologna (<https://cris.unibo.it/>).  
When citing, please refer to the published version.

(Article begins on next page)

This is the final peer-reviewed accepted manuscript of:

**J Microsc. 2020 Mar;277(3):160-169.**

**Epub 2019 Aug 2.**

**Hierarchical electrospun tendon-ligament bioinspired scaffolds induce changes in fibroblasts morphology under static and dynamic conditions**

A Sensini, L Cristofolini, A Zucchelli, M L Focarete, C Gualandi, A DE Mori, A P Kao, M Roldo, G Blunn, G Tozzi

**PMID: 31339556 DOI: 10.1111/jmi.12827**

The final published version is available online at:

<https://doi.org/10.1111/jmi.12827>

Rights / License:

The terms and conditions for the reuse of this version of the manuscript are specified in the publishing policy. For all terms of use and more information see the publisher's website.

# Hierarchical electrospun tendon-ligament bioinspired scaffolds induce changes in fibroblasts morphology under static and dynamic conditions

Alberto Sensini<sup>1</sup>, Luca Cristofolini<sup>1,2</sup>, Andrea Zucchelli<sup>1</sup>, Maria Letizia Focarete<sup>2,3</sup>, Chiara Gualandi<sup>3,4</sup>, Arianna De Mori<sup>5</sup>, Alexander Kao<sup>6</sup>, Marta Roldo<sup>5</sup>, Gordon Blunn<sup>5</sup>, Gianluca Tozzi<sup>6</sup>

- <sup>1</sup> Department of Industrial Engineering, Alma Mater Studiorum—University of Bologna, I-40131 Bologna, Italy
- <sup>2</sup> Health Sciences and Technologies—Interdepartmental Center for Industrial Research (CIRI-HST), Alma Mater Studiorum—University of Bologna, I-40064 Ozzano dell’Emilia, Bologna, Italy
- <sup>3</sup> Department of Chemistry ‘G. Ciamician’ and National Consortium of Materials Science and Technology (INSTM, Bologna RU), Alma Mater Studiorum—University of Bologna, I-40126 Bologna, Italy
- <sup>4</sup> Advanced Mechanics and Materials – Interdepartmental Center for Industrial Research (CIRI-MAM), Alma Mater Studiorum—University of Bologna, I-40123 Bologna, Italy
- <sup>5</sup> School of Pharmacy and Biomedical Science, University of Portsmouth – St Michael’s Building, White Swan Road, Portsmouth PO1 2DT, United Kingdom
- <sup>6</sup> Zeiss Global Centre, School of Mechanical and Design Engineering, University of Portsmouth, Portsmouth PO1 3DJ, United Kingdom

***Corresponding author:***

Gianluca Tozzi  
Zeiss Global Centre  
School of Mechanical and Design Engineering  
University of Portsmouth  
PO1 3DJ Portsmouth, United Kingdom  
e-mail: gianluca.tozzi@port.ac.uk

## 1 **Summary**

2 The regeneration of injured tendons and ligaments is challenging since the scaffolds  
3 needs proper mechanical properties and a biomimetic morphology. In particular, the  
4 morphological arrangement of scaffolds is a key point to drive the cells growth to  
5 properly regenerate the collagen extracellular matrix. Electrospinning is a promising  
6 technique to produce hierarchically structured nanofibrous scaffolds able to guide cells  
7 in the regeneration of the injured tissue. Moreover, the dynamic stretching in bioreactors  
8 of electrospun scaffolds had demonstrated to speed up cell shape modifications *in vitro*.  
9 The aim of the present study was to combine different imaging techniques such as high-  
10 resolution x-ray tomography (XCT), scanning electron microscopy (SEM), fluorescence  
11 microscopy and histology to investigate if hierarchically structured poly(L-lactic acid)  
12 and collagen electrospun scaffolds can induce morphological modifications in human  
13 fibroblasts, while cultured in static and dynamic conditions. After 7 days of parallel  
14 cultures, the results assessed that fibroblasts had proliferated on the external nanofibrous  
15 sheath of the static scaffolds, elongating themselves circumferentially. The dynamic  
16 cultures revealed a preferential axial orientation of fibroblasts growth on the external  
17 sheath. The aligned nanofiber bundles inside the hierarchical scaffolds instead, allowed  
18 a physiological distribution of the fibroblasts along the nanofiber direction. Inside the  
19 dynamic scaffolds, cells appeared thinner compared with the static counterpart. This  
20 study had demonstrated that hierarchically structured electrospun scaffolds can induce  
21 different fibroblasts morphological modifications during static and dynamic conditions,  
22 modifying their shape in the direction of the applied loads.

23



24 **Keywords:**

25 Electrospinning, Hierarchical Scaffolds, High-Resolution X-Ray Tomography, Cell  
26 Culture, Dynamic Cell Culture, Cell Morphology, Tissue Engineering, Tendons and  
27 Ligaments.

28

29 **Introduction**

30 The challenge of the innovative three-dimensional scaffolds, suitable for tendon and  
31 ligament regeneration, is to strictly reproduce the native tissue mechanical properties  
32 and hierarchical morphology (Alshomer et al., 2018; Cheng et al., 2015; Goulet et al.,  
33 2014; Kuo et al., 2010). The morphological arrangement of the scaffold is fundamental  
34 to correctly drive cell proliferation and growth, during collagen extracellular matrix  
35 regeneration. It has been shown that fibroblasts and tenocytes shape is strictly dependent  
36 on the specific site of growth *in vivo*: cells that colonize tendon and ligament membranes  
37 (made of randomly arranged collagen fibrils), tend to spread their bodies; conversely,  
38 cells in the internal volume of these tissues appear elongated in the direction of the  
39 axially oriented fibrils (Kannus, 2000; Kastelic et al., 1978; Murphy et al., 2016).  
40 Several manufacturing approaches to produce fibrous scaffolds inspired to tendons or  
41 ligaments have been investigated in literature, among these electrospinning technology  
42 is the most promising (Sensini & Cristofolini, 2018). Thanks to the possibility to obtain  
43 nanoscale fibers with different spatial arrangements, electrospun scaffolds have  
44 demonstrated enhancement of cellular orientation in the fibers direction (Bosworth &  
45 Downes, 2011; Denchai et al., 2018). Furthermore, several studies have confirmed the  
46 possibility to speed up cell proliferation and elongation on the electrospun scaffolds with  
47 a simplified shape, such as flat mats, bundles or yarns, by uniaxially stretching the  
48 constructs in a bioreactor (Bosworth et al., 2014; Wu et al., 2017; Xu et al., 2014;  
49 Youngstrom & Barrett, 2016). These simple designs allow for convenient  
50 documentation of changes in cellular shape using standard techniques, such as scanning  
51 electron microscopy (SEM), fluorescent microscopy or histology. Despite the high-  
52 quality of images and the cellular information obtainable, these gold-standard methods  
53 have shown some limitation when applied to the study of the cell morphology on

54 complex three-dimensional scaffolds (Leferink et al., 2016). SEM images can achieve a  
55 high-resolution, but are limited to the surface of the structures. Fluorescent techniques,  
56 such as fluorescent or confocal microscopy, allow an accurate identification of the shape  
57 of cells, but are strongly limited by possible autofluorescent effects of the nanofibers,  
58 especially if they are composed by natural polymers such as collagen (Sensini et al.,  
59 2018). Moreover, these techniques do not allow easy visualization if the structure  
60 investigated is not planar, making the investigation of three-dimensional scaffolds  
61 challenging. On the other hand, histology allows a clear identification of the cellular  
62 components, even in case of three-dimensional shapes, but it typically produces a bi-  
63 dimensional view of the specimens and of the cells inside. This limits a correct definition  
64 of the cellular shape. Moreover, during the slicing and washing procedure, in particular  
65 for the electrospun materials, it is easy to damage parts of the scaffold losing the related  
66 information. A possible solution to overcome these limitations is offered by high-  
67 resolution x-ray computed tomography (XCT). However, due to the low X-ray  
68 attenuation of the polymeric nanofibers, XCT investigation of electrospun materials is  
69 particularly challenging. This problem is especially true in the case of collagenous  
70 materials (Balint et al., 2016; Zidek et al., 2016). Recent studies have defined dedicated  
71 protocols to overcome such limitations even in case of submicron voxel sizes (Bosworth  
72 et al., 2014; Sensini et al., 2018). Furthermore, Bradley et al. have defined a procedure  
73 to document, by using a laboratory XCT, cell infiltration inside electrospun mats of  
74 random microfibers (Bradley et al., 2017). However, to the best of our knowledge, no  
75 work has ever tried to investigate the cell growth and infiltration in complex three-  
76 dimensional electrospun nanofibrous scaffolds by combining XCT and other different  
77 imaging techniques. This approach could be fundamental to analyze how the different  
78 elements of the scaffolds can induce cellular morphological modifications.

79 The aim of the present study was to compare the fibroblast morphological modifications  
80 during static and dynamic culture protocols on complex electrospun scaffolds. Cells  
81 were seeded on three-dimensional electrospun nanofibrous hierarchically structured  
82 scaffolds made of a poly(*L*-lactic acid) (PLLA) and collagen (Coll) blend. Different  
83 imaging techniques including high-resolution x-ray tomography (XCT), scanning  
84 electron microscopy (SEM), fluorescent microscopy and histology were employed  
85 confirming different cellular modifications in shape and orientation during static and  
86 dynamic conditions of culture.

## 87 **Materials and methods**

88 In order to investigate the morphologically changes in the fibroblasts shape, electrospun  
89 PLLA/Coll nanofibrous hierarchically structured scaffolds were produced (Figure  
90 1(A)). The scaffolds were seeded with human fibroblasts and cultured in different  
91 conditions for 7 days: two of each in static conditions, while the other two were stretched  
92 two times in a bioreactor for 1 hour each (Figure 1(B)). At the end of the culture, the  
93 specimens were cut in pieces and investigated with different imaging techniques (Figure  
94 1(C)).

### 95 *Hierarchical electrospun scaffolds production*

96 In order to reproduce the morphology of tendon and ligament fibrils and fascicles  
97 (Kannus, 2000; Murphy et al., 2016), electrospun bundles (cross-sectional diameter =  
98 550-650  $\mu\text{m}$ ) of aligned nanofibers (cross-sectional diameter of the nanofibers =  
99  $0.36\pm 0.06 \mu\text{m}$ ) of a PLLA/Coll-75/25 (w/w) blend were produced as previously  
100 described (Sensini et al., 2017, 2018). To obtain the bundles the following  
101 electrospinning parameters were used: a rotating drum collector (peripheral speed = 22.8  
102  $\text{m s}^{-1}$ ); the polymer solution was delivered through two needles (internal diameter 0.51

103 mm); room temperature (RT) and relative humidity 20–30%; applied voltage = 22 kV;  
104 feed rate = 0.5 mL h<sup>-1</sup>, electrospinning time = 2 hours; needles-collector distance = 200  
105 mm; the sliding spinneret with the two needles had an excursion of 120 mm, with a  
106 sliding speed of 1200 mm min<sup>-1</sup>.

107 To reproduce the structure of a whole tendon or ligament (Kastelic et al., 1978; Murphy  
108 et al., 2016), each bundle was pulled out from the drum, obtaining a ring-shaped  
109 structure that was twisted in the middle and bent over itself. Then, each assembly was  
110 covered with an electrospun epitenon/epiligament-like sheath, as previously described  
111 (WO 2018/229615 A1, 2018; Sensini et al., 2019; Sensini et al., 2019). The scaffolds  
112 were finally crosslinked with a mixture of *N*-(3-dimethylaminopropyl)-*N'*-  
113 ethylcarbodiimide hydrochloride (EDC) and *N*-hydroxysuccinimide (NHS) (Sigma-  
114 Aldrich, USA) as previously described (Alberto Sensini et al., 2018) (cross-sectional  
115 diameter = 1.46±0.08 mm; length of the scaffolds = 89.4±2.1 mm). Four hierarchical  
116 scaffolds were produced (Figure 1).

#### 117 *Cell seeding*

118 The four hierarchical scaffolds were sterilized by immersion in 70% (v/v) ethanol (Acros  
119 Organics, Thermo Fisher Scientific, BEL) for 1 hour, washed in sterile PBS (Thermo  
120 Fisher Scientific, USA) three times to remove any remaining ethanol and equilibrated in  
121 complete medium for 24 hours. The complete medium was obtained by mixing  
122 Dulbecco Modified Eagle Medium (DMEM) (i.e. 4.5 g/L D-Glucose, with  
123 GlutaMAX™ and Pyruvate) (Thermo Fisher Scientific, USA), 10% foetal bovine serum  
124 (Thermo Fisher Scientific, USA) and 1% (v/v) penicillin/streptomycin solution (Thermo  
125 Fisher Scientific, USA).

126 Human foreskin fibroblasts (Hs27) were cultivated with complete medium at 37°C in a  
127 humid atmosphere with 5% CO<sub>2</sub>. Medium was refreshed three times a week and cells  
128 were used between passage 4 and 6.

129 To perform the test, cells were seeded at  $2.0 \times 10^5$  cells/scaffold. In particular, cells were  
130 suspended in 350 microliters of complete medium and seeded, using a syringe with a  
131 25G needle: half volume was seeded on one side of the scaffold, then the scaffold was  
132 turned 180° and the other half volume was seeded on the other side. The seeding was  
133 carried out in a sterile petri dish. After 45 minutes in an incubator at 37°C and 5% CO<sub>2</sub>,  
134 each hierarchical scaffold was transferred into one low adherence T25 flask each and  
135 covered with 5 ml of complete medium to allow for cell proliferation.

136 In order to avoid potential artefacts caused by the relevant amount of medium during the  
137 dynamic cultures (see below) and the total length of the specimens, quantitative data  
138 regarding the cell viability were not reported.

139 After 7 days of culture, the hierarchical scaffolds were fixed for 48 hours in 4%  
140 paraformaldehyde (PFA, Sigma-Aldrich, Saint Louis, USA) in PBS (at 4°C). Then, each  
141 specimen was cut in the center and divided in two equal sections: one half for the  
142 SEM/XCT imaging; the other was cut in two additional pieces for fluorescence  
143 microscopy and histology (Figure 1(C)).

#### 144 *Dynamic cultures in bioreactor*

145 The dynamic culture was carried out on two hierarchical scaffolds by using a  
146 commercial bioreactor (MCB1, CellScale, CAN). Before each stretching session, the  
147 bioreactor was sterilized by washing the test chamber in ethanol 70% (v/v) and sterilized  
148 by means UV radiations under a fume hood for an hour. To transmit a uniaxial  
149 stretching, the hierarchical scaffolds were hooked between the stainless-steel actuator of

150 the bioreactor and a custom-made 3D printed pin of acrylonitrile butadiene styrene  
151 (ABS) (ABS-M30, Stratasys, USA). During each session, the specimens were covered  
152 with 150 ml of complete medium and stimulated for 1 hour with 4 mm of displacement  
153 (corresponding at a strain of approximately 5%) at a frequency of 1 Hz (3600 cycles).  
154 These parameters were chosen in accordance with the literature (Bosworth et al., 2014).  
155 Each of the two scaffolds was stretched two times during the 7 days of culture (i.e. at  
156 day three and day six of culture). After each bioreactor session, the dynamic specimens  
157 were put in T25 flasks with 5 ml of medium and left in static conditions for two days.

#### 158 *Static cultures*

159 Parallely, as a control for the dynamic specimens, two hierarchical scaffolds were  
160 cultured for 7 days in T25 flasks with 5 ml of medium, changing the medium at day 3  
161 and six of culture.

#### 162 *High-resolution x-ray tomography*

163 To evaluate the full-field fibroblast distribution, morphology and the hierarchical  
164 arrangement in the scaffolds, an XCT investigation was performed.

165 Firstly, after fixing with PFA, the scaffolds specimens for XCT were washed three times  
166 in PBS. Specimens were post-fixed with osmium tetroxide (Sigma-Aldrich, USA) for 1  
167 hour and then dehydrated in ethanol (v/v) 30%, 50%, 70%, 90%, 95% and 100% for 1  
168 hour for each step (the 100% step was repeated twice). Then the specimens were  
169 dehydrated in acetone for 20 minutes. The specimens were chemically dried using a  
170 mixture of hexamethyldisilazane (HMDS) (Sigma-Aldrich, USA) and ethanol in  
171 different (v/v) ratios: (i) HMDS:ethanol = 1:2 (v/v) and (ii) HMDS:ethanol = 2:1 (v/v)  
172 for 20 minutes each. An additional step was performed in HMDS 100% until dry.

173 To avoid imaging artifacts resulting from micromovements, the specimens were fixed  
174 in custom-made plastic masks adapted from (Sensini et al., 2018).

175 The two dynamic and static specimens of the hierarchical scaffolds were scanned with  
176 a laboratory XCT system (Xradia 520 Versa, Zeiss X-ray Microscopy, USA), with the  
177 following parameters:

178 (i) Voxel size = 1.6 micrometers (i.e. overview of the specimens): 40 kV voltage, 2  
179 W power, 49 microampere tube current, 10 sec. exposure time.

180 (ii) Voxel size = 0.5 micrometers (i.e. zoom-in on the fibroblasts): 40 kV voltage, 2  
181 W power, 50 microampere tube current, 30 sec. exposure time.

182 All the XCT images, were reconstructed using the Scout-and-Scan Reconstructor  
183 software (Zeiss, USA), and were visualized using XM3DViewer1.2.8 software (Zeiss,  
184 USA).

### 185 *SEM imaging*

186 After the XCT investigation, in order to confirm the fibroblasts presence, the XCT  
187 specimens were removed from the masks and prepared for the SEM imaging. Each  
188 specimen was cut in two pieces: one was longitudinally opened with a scalpel to  
189 investigate the fibroblasts on the internal bundles, while the other was left intact to  
190 investigate the fibroblasts on the electrospun sheath. Scanning Electron Microscopy  
191 (SEM) (Philips 515 SEM, NL) observations were carried out using an accelerating  
192 voltage of 15 kV and specimens were gold sputtered.

### 193 *Directionality analysis*



194 In order to quantify the orientation of the nanofibers of the scaffolds, the Directionality  
195 plugin of ImageJ was used (Liu, 1991; Schindelin et al., 2012; Schneider et al., 2012).  
196 This approach quantifies the distribution of nanofibers within a given angle from the  
197 axis of the specimen. The analysis was performed using a Local Gradient Orientation  
198 method following a procedure previously applied (Sensini et al., 2018).

199 To assess the orientation of the bundles inside the hierarchical assemblies, a full volume  
200 investigation was performed applying the procedure to all the slices of the XCT stack  
201 (voxel size = 1.6 micrometers), after reslicing. In order to list also the orientation of the  
202 nanofibers in a single crosslinked PLLA/Coll-75/25 bundle, the Directionality analysis  
203 data on a XCT scan from a previous study were reported (Sensini et al., 2018).

204 To quantify the orientation of the nanofibers in the electrospun sheath the Directionality  
205 analysis was performed on a stack of 5 SEM surface images (magnification = 8000x)  
206 derived from (Sensini et al., 2018).

207 In order to investigate the preferential orientation of the fibroblasts on the external  
208 sheath, in static and dynamic conditions of culture, a Directionality investigation was  
209 performed on a stack of 2 fluorescent images for each condition of culture (see below)  
210 (magnification = 20x) derived and adapted from (Sensini et al., 2018; Tseng et al., 2013).

211 As the nuclei are better visible and are stretched in the same direction of the cell itself,  
212 the analysis was based on the alignment of the nuclei. Firstly, to enhance visibility of  
213 the cells nuclei the fluorescent images were segmented, using ImageJ. Over each  
214 segmented image, a mask was produced onto which lines were drawn of the same length  
215 and orientation of the longest axis of each nucleus. Finally, the masks were analyzed  
216 with Directionality as described above.

217 *Fluorescent microscopy*

218 After PFA fixing, specimens were washed with PBS and put in 3 ml of Triton-X (Sigma-  
219 Aldrich, USA) 0.1% (v/v) for 15 min. Then, the scaffolds were washed 3 times with  
220 PBS, before being treated with 1% (v/v) bovine serum albumin (BSA) (Sigma-Aldrich,  
221 USA) in PBS, for 1 hour. Then, the specimens were washed twice with sterile PBS.  
222 Phalloidin Dylight 550 (Thermo Fisher Scientific, USA) (2 units/ml in PBS) was added  
223 to each sample before incubation for 90 min at RT. Then the specimens were washed  
224 two times with PBS and DAPI (Sigma Aldrich, USA) (2 µg/ml) was added and  
225 incubated for 20 min in the dark, at RT. The specimens were stored at 4°C in petri dishes  
226 containing sterile PBS to prevent specimen dehydration. Finally, the external surfaces  
227 of the were imaged using a fluorescent microscope (Axio Imager Z1, Zeiss, USA)  
228 equipped with a camera (Hamamatsu HR, Hamamatsu, JAP) and a color camera  
229 (AxioCam MRc, Zeiss, USA) too. Images were processed by Volocity 6.3 software  
230 (Quorum Technologies Inc, UK).

### 231 *Histology*

232 The specimens for the haematoxylin and eosin staining were fixed in 4% (v/v) PFA/PBS  
233 overnight. PFA fixed specimens were processed into paraffin (Histosec®, Merck,  
234 Darmstadt, GER), using a dedicated embedder (EG1150 H, Leica, Wetzlar, GER) and  
235 sectioned (slices thickness = 5 µm) using a microtome (RM2235, Leica, GER). The  
236 specimens were sectioned parallelly to their longitudinal axis. Sections were  
237 deparaffinized and incubated in hematoxylin (Sigma-Aldrich, USA) and then in  
238 alcoholic eosin (Sigma-Aldrich, USA) for 5 min respectively. Finally, sections were  
239 differentiated, dehydrated in graded series of ethanol, and mounted in dibutyl phthalate  
240 xylene (DPX) (Sigma-Aldrich, USA) using glass coverslips. The histological slices of  
241 the scaffolds were imaged using a microscope (Diaplan, Leitz, GER) and processed with  
242 the Image-Pro Plus 6 software (Media Cybernetics, UK).

## 243 *Cell morphology*

244 In order to quantify the dimensions of cells (the length, i.e. the preferential direction of  
245 elongation of the cellular body; and the width and thickness), in the different conditions  
246 of culture, measurements of cells bodies were performed using ImageJ on the different  
247 images acquired. The cells length and width were estimated from XCT, fluorescence,  
248 SEM and histological images (static cultures: n = 20 cells for the length; n = 27 cells for  
249 the width; dynamic cultures: n = 8 cells for the length; n = 4 cells for the width), while  
250 the cells thickness was measured using SEM and histological images (static cultures: n  
251 = 7 cells; dynamic cultures: n = 5 cells). The mean (three measurements for each cell)  
252 of each parameter was used to produce the final mean and standard deviation of each  
253 dimension.

## 254 **Results**

### 255 *Morphological investigation of the hierarchical scaffolds*

256 To investigate the orientation of the nanofibers and bundles in the different levels of the  
257 hierarchical scaffolds, a Directionality analysis was performed (Figure 2). The  
258 Directionality analysis confirmed the preferential axial orientation of the nanofibers in  
259 the bundles, with a predominant peak of  $31.4 \pm 2.82\%$  in the range of  $0^\circ$ - $3^\circ$  from the  
260 bundle axis, and a decrescent distribution (Sensini et al., 2018). A small amount of  
261 nanofibers ( $0.55 \pm 0.08\%$ ) was perpendicular to the bundle ( $87^\circ$ - $90^\circ$ ). The Directionality  
262 investigation showed that the nanofibers of the sheaths for the hierarchical assemblies  
263 had a slight preferential circumferential orientation: more than 31% of the nanofibers  
264 fell in the range of  $66^\circ$ - $90^\circ$ . The preferential axial of alignment of the bundles inside the

265 hierarchical scaffolds was confirmed by a predominant peak of  $61.6\% \pm 9.43\%$  in the  
266 range of  $0^\circ$ - $3^\circ$ , and a decrescent distribution.

### 267 *Fibroblasts morphology from XCT investigation*

268 The specimens mounting setup for the XCT scans successfully prevented the artefacts  
269 of micromovements, permitting to obtain high-resolution images after the three-  
270 dimensional reconstruction (Figure 3). The hierarchical scaffolds were homogeneous,  
271 and the internal bundles strongly grouped by the electrospun sheath. The cells fixation  
272 and dehydration procedure enabled visualization of the fibroblasts growth on the  
273 hierarchical scaffolds (Figure 3). The reconstructions with a  $1.6 \mu\text{m}$  voxel size provided  
274 an overview of the specimens (Figure 3(A)). Zooming on the sheath at  $0.5 \mu\text{m}$  voxel  
275 size, fibroblasts were clearly distinguishable (Figure 3(B)). On the sheath of static  
276 specimens, fibroblasts were circumferentially oriented along the axis of the scaffolds,  
277 **spreading their bodies also** along the scaffold longitudinal axis (Figures 3(AI, AII) and  
278 3(BI, BII)). On the sheath of dynamic specimens, the fibroblasts were **thinner and less**  
279 **wide (see below)**, with increasing axial orientation compared to the static ones (Figure  
280 3(AIII, AIV) and 3(BIII, BIV)). In the internal bundles, due to the high-alignment of the  
281 nanofibers and the elongated shape of the fibroblasts, cell detection was not possible.

### 282 *Fibroblasts morphology from SEM investigation*

283 The SEM images obtained for the same specimens used for the XCT scans and are  
284 shown in Figure 4. Despite the preferential random arrangement of the sheath  
285 nanofibers, the static fibroblasts showed a circumferential orientation with spread bodies  
286 (Figure 4(AI, II)), while cells on the dynamic specimens were thinner and preferentially  
287 elongated axially to the hierarchical scaffolds (Figure 4(BI, II)). The SEM investigation  
288 also assessed the fibroblasts infiltration inside the hierarchical scaffolds, both in static

289 and dynamic conditions. In both test conditions the internal fibroblasts appeared  
290 elongated and distributed axially aligned with the bundles nanofibers (Figure 4(AIII,  
291 AIV) and (BIII, BIV)). In the dynamic specimens the fibroblast appeared thinner  
292 compared to the static counterpart (Figure 4(BIII, IV)).

### 293 *Fibroblasts morphology from fluorescence microscopy investigation*

294 The fluorescence microscopy results are reported in Figure 5. On the static specimens,  
295 fibroblasts were again circumferentially oriented on the nanofibrous sheath (the nuclei  
296 were also ovalized in the transversal direction of the scaffolds), with spread bodies  
297 (Figure 5(A)). In the sheath of dynamic specimens, the fibroblasts appeared more axially  
298 aligned compared with the static ones (Figure 5(B)).

299 The Directionality analysis of the cell nuclei performed on the electrospun sheaths  
300 revealed that, in static specimens, the 71.1% of cells were oriented in a range of 72°-90°  
301 (Figure 6). In the dynamic specimens instead, the 53.4% of cells were oriented in the  
302 range of 0°-18° (Figure 6).

303 The fluorescence investigation in the internal bundles was not possible due to a low  
304 infiltration of the fluorescent reagents.

### 305 *Fibroblasts morphology from histological investigation*

306 The histological investigation outcomes are showed in Figure 6. The axial slices of the  
307 hierarchical scaffolds obtained, had cut transversally the fibroblasts grown on the  
308 electrospun sheaths (Figure 7(AI, II) and 7(BI, II)). In both the static and dynamic  
309 specimens, the fibroblasts appeared preferentially circumferentially arranged, due to the  
310 reduced axial elongation of their bodies. Moreover, on the dynamic specimens, the  
311 fibroblasts were thinner than on the static ones (according to their progressive extension

312 in the axial direction). Cells also infiltrated inside the hierarchical scaffolds aligning  
313 themselves in the nanofibers direction (Figure 7(AIII, IV) and 7(BIII, IV)). The  
314 fibroblasts in the dynamic specimens appeared thinner compared with the static  
315 counterpart.

#### 316 *Quantification of cells morphology*

317 The quantification of cells morphology revealed that in the static specimens, the cells  
318 on the electrospun sheaths had a length of  $72.1 \pm 27.9$  micrometers, a width of  $18.8 \pm 15.3$   
319 micrometers and a thickness of  $3.2 \pm 0.8$  micrometers; in the internal bundles, the cells  
320 showed a length of  $26.8 \pm 9.9$  micrometers, a width of  $2.5 \pm 1.6$  micrometers and a  
321 thickness of  $1.5 \pm 0.2$  micrometers. In the dynamic specimens, the cells on the sheath had  
322 a length of  $77 \pm 52.4$  micrometers, a width of  $8.9 \pm 6.9$  micrometers and a thickness of  
323  $1.9 \pm 0.6$  micrometers; on the internal bundles the cells had a length of  $21.4 \pm 8.5$   
324 micrometers, a width of  $2.6 \pm 1.3$  micrometers and a thickness of  $1.2 \pm 0.8$  micrometers.

#### 325 **Discussion**

326 To produce an electrospun scaffold suitable for tendon and ligament tissue engineering,  
327 proper mechanical properties need to be combined to a biomimetic hierarchical  
328 structure. These properties are mandatory to transmit physiological loads to the cells,  
329 enabling their proper infiltration and growth inside the scaffolds. The aim of this study  
330 was to investigate an innovative electrospun PLLA/Coll-75/25 hierarchically structured  
331 scaffold, using different imaging techniques, in order to evaluate its ability to guide the  
332 fibroblasts growth in static and dynamic conditions. The hierarchical scaffolds were  
333 assembled by wrapping a PLLA/Coll-75/25 ring-shaped bundles of axially aligned  
334 nanofibers, with an electrospun PLLA/Coll-75/25 sheath of randomly oriented

335 nanofibers. The scaffolds nanofibers and bundles were in the same size range of collagen  
336 fibrils and fascicles reported in literature (Kastelic et al., 1978). The Directionality  
337 analysis confirmed that bundles nanofibers, as well as bundles themselves, were axially  
338 aligned with the hierarchical scaffolds, while the nanofibers of the sheath showed a  
339 slightly circumferential orientation (Figure 2). In this way the hierarchical structure of a  
340 whole tendon or ligament was reproduced (Kastelic et al., 1978; Murphy et al., 2016).  
341 In order to evaluate the morphological changes in the cell shape induced by the  
342 hierarchical scaffolds, Hs27 fibroblasts were seeded on them for 7 days, comparing a  
343 static culture with a dynamic one in a bioreactor. To reproduce a physiological  
344 displacement configuration, the stretching parameters of the bioreactor were chosen  
345 consistently with the previous literature (Bosworth et al., 2014). At the end of the  
346 cultures, the full-field XCT investigation permitted to successfully visualize the  
347 fibroblasts grown on the external sheaths (Figure 3). Considering such complex and  
348 three-dimensional nanofibrous scaffolds, acquiring XCT images was challenging. In  
349 their work, Bradley et al. (Bradley et al., 2017) were able to visualize human fibroblasts  
350 seeded on electrospun poly(lactide-*co*-glycolide) (PLGA) random microfibrinous mats by  
351 using a laboratory XCT scanner thanks to the micrometric cross-section of the fibers and  
352 the different levels the X-rays attenuation between the PLGA and the cellular  
353 component. In the case of the PLLA/Coll nanofibers instead, it is difficult to obtain  
354 tomographic images fibers, due to the low absorption of the collagen of X-rays (Balint  
355 et al., 2016; Zidek et al., 2016). This criticality is increased when the aim of the XCT  
356 scan is to discriminate elements with a similar attenuation and dimensions, such as cells  
357 and collagenous nanofibers. This aspect was fundamental for the XCT visualization of  
358 fibroblasts. Due to their spread shape and the random arrangement of the nanofibers,  
359 fibroblasts detection on the electrospun sheath was clearly visible (Figure 3(B)).

360 Conversely, the identification of cells inside the internal bundles was not distinguishable  
361 (Figure 3(AII) and 3(AIV)). This was mainly caused by the axially aligned nanofibers  
362 and the thinner and elongated shape of the cells. Further optimization, especially in the  
363 thresholding phase would possibly to allow the XCT detection of cells along the bundles  
364 aligned nanofibers.

365 In order to overcome this limitation and to validate the XCT results, additional imaging  
366 techniques such as fluorescence microscopy, SEM and histology were performed. The  
367 combination of these imaging protocols confirmed that fibroblasts on the electrospun  
368 sheath of the scaffolds adopt a different shape depending on the culture conditions  
369 employed. Both on the static and on the dynamic specimens, the cells had a length that  
370 was one order of magnitude longer than the other two dimensions. On the electrospun  
371 sheath of the static specimens, cells were elongated along the circumference of the  
372 scaffolds with a spread body, while in the dynamic ones, a prevalent axial orientation  
373 with thinner and slender morphology was observed (Figures 3-5 and Figure 7).

374 Moreover, the SEM and histological investigations showed that fibroblasts were able to  
375 penetrate inside the electrospun sheath, growing and aligning themselves in the direction  
376 of the axially aligned nanofibers. In the dynamic specimens, the cells bodies were  
377 slightly thinner and shorter (length =  $21.4 \pm 8.5$  micrometers; thickness =  $1.2 \pm 0.8$   
378 micrometers) compared to the static ones (length =  $26.8 \pm 9.9$  micrometers; thickness =  
379  $1.5 \pm 0.2$  micrometers) (Figures 4, 5 and Figure 7). These results were in accordance with  
380 the previous studies on cell cultures carried out on PLLA/Coll electrospun bundles of  
381 aligned nanofibers (Sensini & Cristofolini, 2018; Sensini et al., 2018).

382 However, considering the different imaging investigations, the fibroblasts grown on the  
383 sheath of the hierarchical scaffolds showed an unprecedented phenomenon compared to  
384 previous cell studies (Alshomer et al., 2018; Hampson et al., 2008; Sensini &



385 Cristofolini, 2018). In fact, the circumferential alignment and elongation of cells grown  
386 in the static condition was unexpected, even considering the slightly circumferential  
387 alignment of the sheath nanofibers (Figure 2). Moreover, when cultured under dynamic  
388 conditions, the sheath fibroblasts progressively elongated their shape trying to align  
389 themselves to the axis of the hierarchical scaffolds. All these qualitative considerations  
390 about the cellular orientation, were confirmed by the cellular Directionality analysis  
391 performed on cells grown on the sheaths in the different conditions of culture (Figure  
392 6). This behavior can be probably ascribed to the combination of three factors: the  
393 electrospinning production process of the sheath, the hydration and mechanical  
394 component, and the crosslinking of the nanofibers. Firstly, the mechanism to produce  
395 the sheath was proved to tune the level of compacting of the internal bundles of the  
396 hierarchical scaffolds (WO 2018/229615 A1, 2018; Sensini et al., 2019; Sensini et al.,  
397 2019). This effect causes a pre-tensioning of the sheath nanofibers and of the internal  
398 bundles. Secondly, after immersion in the culture medium, the scaffolds absorbed the  
399 liquid which likely resulted in swelling of the internal bundles inducing additional  
400 stretching of the sheath. The combination of these two effects can explain the presence  
401 of circumferential stress, that could in turn drive the fibroblasts to change shape even in  
402 static conditions. The progressive axial alignment of cells in the dynamic cultures  
403 instead, could be explained by considering the effect of the collagen crosslinking. In  
404 fact, it is possible that, during the crosslinking process, the nanofibers at the interface  
405 between the sheath and the internal bundles could have been crosslinked together,  
406 reducing their sliding. This could have caused a transmission of the axial load between  
407 the bundles and sheath, producing an increment of the longitudinal stretch of the sheath  
408 themselves, that induced the cells alignment. Both these effects, to the best of our

409 knowledge, were completely unexplored so far and they need further investigations in  
410 the near future increasing the sample size of the hierarchical scaffolds tested.

## 411 **Conclusion**

412 In this study a preliminary investigation on the change in fibroblasts morphology was  
413 assessed by culturing them on electrospun hierarchical scaffolds in static and dynamic  
414 conditions. The integration between XCT scans and gold-standard techniques such as  
415 SEM, fluorescence microscopy and histology allowed the detection of the modifications  
416 in the cell morphology and orientation. Considering the results, these electrospun  
417 hierarchical scaffolds could be suitable for future *in vivo* animal study, permitting an  
418 axial orientation of cells both on the electrospun sheath and the internal bundles when  
419 stimulated with axial loads. Moreover, the improvement of the imaging protocols  
420 developed in this study will be useful for the future development of correlative  
421 microscopy workflows dedicated to similar electrospun materials.

## 422 **Acknowledgments**

423 The Italian Ministry of University and Research (MIUR) is acknowledged. The mobility  
424 of Alberto Sensini was funded by the University of Bologna (Marco Polo grant). Type I  
425 collagen was kindly provided by Kensey Nash Corporation d/b/a DSM Biomedical  
426 (Exton, USA). The Zeiss Global Centre at the University of Portsmouth is greatly  
427 acknowledged for the support in X-ray imaging and data post-processing. The project  
428 was partially funded by the University of Portsmouth through a Research and Innovation  
429 Development Fund. The authors greatly acknowledge CellScale and Jim Veldhuis for  
430 technical training of Alberto Sensini in the use of the bioreactor. The authors  
431 acknowledge Carlo Gotti and Marina Fichera for the help during the scaffolds  
432 production and the imaging post processing. Marco Curto, Martino Pani and Robin

433 Rumney were also gratefully acknowledged for the help and suggestions in the design  
434 of the 3D-printed parts, design tables reviewing, and the cell culture planning. The  
435 authors also gratefully acknowledge Sabrina Valente and Gianandrea Pasquinelli for the  
436 useful suggestions and the use of the facilities during the histologic investigations.

### 437 **Figure captions**

438 **Fig. 1.** Workflow of the experiment. (A) Electrospun hierarchical scaffolds assembly  
439 (scale bar = 1 mm). (B) Fibroblasts culture: two scaffolds were cultured in static  
440 conditions, while other two with uniaxial sessions of stretching in a bioreactor. (C)  
441 Scaffolds preparation for the different imaging investigations (scale bar = 1 mm).

442 **Fig. 2.** Directionality analysis at different levels of the hierarchical scaffolds. The  
443 directionality histograms show the comparison between: the alignment of the bundles  
444 inside the hierarchical scaffold (gray bars), the distribution of nanofibers in the different  
445 directions for the bundle (green bars) and on the electrospun sheath (blue bars). An angle  
446 of  $0^\circ$  means that the nanofibers were aligned with the longitudinal axis of the  
447 hierarchical scaffold, an angle of  $90^\circ$  means that the nanofibers were perpendicular to it.  
448 Mean and standard deviation between images of the same specimen are plotted.

449 **Fig. 3.** XCT images of fibroblasts cultured onto the hierarchical scaffolds in static (I,  
450 II) and dynamic (III, IV) conditions. (AI, III) Overview of the scaffolds; (AII, IV)  
451 superficial crop showing the internal bundles (voxel size = 1.6 micrometers; scale bar  
452 =1 mm). (BI, III) Overview of fibroblasts on the external sheath; (AII, IV) zoom on the  
453 fibroblasts (voxel size = 0.5 micrometers; scale bar = 200 micrometers).

454 **Fig. 4.** SEM images of fibroblasts cultured onto the hierarchical scaffolds in static (A)  
455 and dynamic (B) conditions (scale bar = 10 micrometers). (I-II) SEM images of the  
456 fibroblasts on the electrospun sheath; (III-IV) SEM fibroblasts on the internal bundles.

457 **Fig. 5.** Fluorescence images of fibroblasts onto the hierarchical scaffolds sheath in static  
458 (A) and dynamic (B) conditions (scale bar = 30 micrometers).

459 **Fig. 6.** Directionality analysis of cells grown on the electrospun sheaths (based on the  
460 orientation of the cells nuclei) in static and dynamic conditions of culture. An angle of  
461  $0^\circ$  means that the cells were aligned with the longitudinal axis of the hierarchical  
462 scaffold, an angle of  $90^\circ$  means that the cells were perpendicular to it. Mean and standard  
463 deviation between images of the static and dynamic specimens are plotted.

464 **Fig. 7.** Histological investigation on the hierarchical scaffolds cultured in static (A) and  
465 dynamic (B) conditions (scale bar = 50 micrometers). (I-II) Zoom-in on the fibroblasts  
466 on the electrospun sheath; (III-IV) images of the elongated fibroblasts on the aligned  
467 nanofibers of the internal bundles.

468

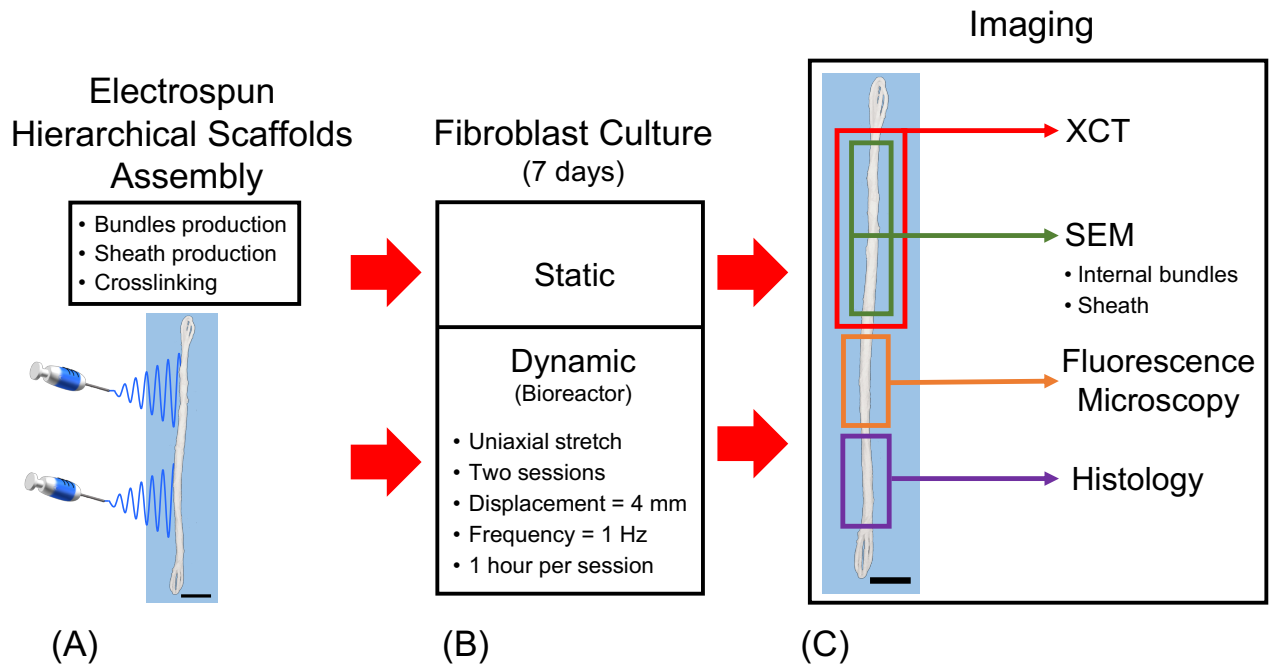
469 **References:**

- 470 Alshomer, F., Chaves, C., & Kalaskar, D. M. (2018). Advances in Tendon and  
 471 Ligament Tissue Engineering : Materials Perspective. *J. Mater.*, **2018**, 1–18.  
 472 <https://doi.org/10.1155/2018/9868151>
- 473 Balint, R., Lowe, T., & Shearer, T. (2016). Optimal contrast agent staining of  
 474 ligaments and tendons for X-ray computed tomography. *PLoS One*, **11**(4).  
 475 <https://doi.org/10.1371/journal.pone.0153552>
- 476 Bosworth, L. A., Rathbone, S. R., Bradley, R. S., & Cartmell, S. H. (2014). Dynamic  
 477 loading of electrospun yarns guides mesenchymal stem cells towards a tendon  
 478 lineage. *J. Mech. Behav. Biomed. Mater.*, **39**, 175–183.  
 479 <https://doi.org/10.1016/j.jmbbm.2014.07.009>
- 480 Bosworth, L. A., & Downes, S. (2011). *Electrospinning for Tissue Regeneration*.  
 481 (Lucy A. Bosworth & S. Downes, Eds.). Cambridge: Woodhead Publishing.  
 482 <https://doi.org/10.1016/B978-1-84569-741-9.50001-X>
- 483 Bradley, R. S., Robinson, I. K., & Yusuf, M. (2017). 3D X-Ray Nanotomography of  
 484 Cells Grown on Electrospun Scaffolds. *Macromol. Biosci.*, **17**(2), 1–8.  
 485 <https://doi.org/10.1002/mabi.201600236>
- 486 Cheng, M. T., Shih, Y. R. V., & Lee, O. K. (2015). Tendon and Ligament Tissue  
 487 Engineering. In A. Vishwakarma, P. Sharpe, S. Shi, & M. Ramalingam (Eds.),  
 488 *Stem Cell Biology and Tissue Engineering in Dental Sciences* (42, 553–565),  
 489 Elsevier Inc. [https://doi.org/https://doi.org/10.1016/B978-0-12-397157-9.00076-](https://doi.org/https://doi.org/10.1016/B978-0-12-397157-9.00076-X)  
 490 X
- 491 Denchai, A., Tartarini, D., & Mele, E. (2018). Cellular Response to Surface  
 492 Morphology: Electrospinning and Computational Modeling. *Front. Bioeng.*  
 493 *Biotechnol.*, **6**(October), 1–11. <https://doi.org/10.3389/fbioe.2018.00155>
- 494 Goulet, F., Auger, F. A., Cloutier, R., Lamontagne, J., Simon, F., Chabaud, S.,  
 495 Germain, L., Hart, D. A. (2014). Tendons and Ligament Tissue Engineering. In  
 496 R. Lanza, R. Langer, & J. Vacanti (Eds.), *Principles of Tissue Engineering* (59,  
 497 1275–1287). Elsevier Inc. <https://doi.org/10.1016/B978-0-12-398358-9.00059-8>
- 498 Hampson, K., Forsyth, N. R., El Haj, A., & Maffulli, N. (2008). Tendon Tissue  
 499 Engineering. In N. Ashammakhi, R. Reis, & F. Chiellini (Eds.), *Topics in Tissue*  
 500 *Engineering* (3, 1–21).  
 501 [https://www.oulu.fi/spareparts/ebook\\_topics\\_in\\_t\\_e\\_vol4/abstracts/hampson.pdf](https://www.oulu.fi/spareparts/ebook_topics_in_t_e_vol4/abstracts/hampson.pdf)
- 502 Kannus, P. (2000). Structure of the tendon connective tissue. *Scand. J. Med. Sci.*  
 503 *Sport.*, **10**(6), 312–320. <https://doi.org/10.1034/j.1600-0838.2000.010006312.x>
- 504 Kastelic, J., Galeski, A., & Baer, E. (1978). The Multicomposite Structure of Tendon.  
 505 *Connect. Tissue Res.*, **6**(1), 11–23. <https://doi.org/10.3109/03008207809152283>
- 506 Kuo, C. K., Marturano, J. E., & Tuan, R. S. (2010). Novel strategies in tendon and  
 507 ligament tissue engineering : Advanced biomaterials and regeneration motifs.  
 508 *Sport. Med. Arthrosc. Rehabil. Ther. Technol.*, **2**(20), 1–14.
- 509 Leferink, A. M., Van Blitterswijk, C. A., & Moroni, L. (2016). Methods of Monitoring  
 510 Cell Fate and Tissue Growth in Three-Dimensional Scaffold-Based Strategies for  
 511 In Vitro Tissue Engineering. *Tissue Eng. Part B Rev.*, **22**(4), 1–19.  
 512 <https://doi.org/10.1089/ten.teb.2015.0340>
- 513 Liu, Z. (1991). Scale space approach to directional analysis of images. *Appl. Opt.*,  
 514 **30**(11), 1369–1373. <https://doi.org/https://doi.org/10.1364/AO.30.001369>
- 515 Murphy, W., Black, J., & Hastings, G. (2016). *Handbook of Biomaterial Properties*.  
 516 (W. Murphy, J. Black, & G. Hastings, Eds.) (Second). Springer.  
 517 <https://doi.org/10.1007/978-1-4939-3305-1>
- 518 Schindelin, J., Arganda-Carreras, I., Frise, E., Kaynig, V., Longair, M., Pietzsch, T., ...

- 519 Cardona, A. (2012). Fiji: an open-source platform for biological-image analysis.  
520 *Nat. Methods*, **9**(7), 676–682. <https://doi.org/10.1038/nmeth.2019>
- 521 Schneider, C. A., Rasband, W. S., & Eliceiri, K. W. (2012). NIH Image to ImageJ: 25  
522 years of image analysis. *Nat. Methods*, **9**(7), 671–675.  
523 <https://doi.org/10.1038/nmeth.2089>
- 524 Sensini, A., Cristofolini, L., Focarete, M. L., Belcari, J., Zucchelli, A., Kao, A., &  
525 Tozzi, G. (2018). High-resolution x-ray tomographic morphological  
526 characterisation of electrospun nanofibrous bundles for tendon and ligament  
527 regeneration and replacement. *J. Microsc.*, **272**(3), 196–206.  
528 <https://doi.org/10.1111/jmi.12720>
- 529 Sensini, A., & Cristofolini, L. (2018). Biofabrication of Electrospun Scaffolds for the  
530 Regeneration of Tendons and Ligaments. *Materials (Basel)*, **11**(10), 1963.  
531 <https://doi.org/10.3390/ma11101963>
- 532 Sensini, A., Cristofolini, L., Gualandi, C., Focarete, M. L., Belcari, J., & Zucchelli, A.  
533 (2018). *WO 2018/229615 A1*.
- 534 Sensini, A., Gotti, C., Belcari, J., Zucchelli, A., Focarete, M. L., Gualandi, C., Todaro,  
535 I., Kao, A. P., Tozzi, G., Cristofolini, L. (2019). Morphologically bioinspired  
536 hierarchical Nylon 6.6 electrospun assembly recreating the structure and  
537 performance of tendons and ligaments. *Med. Eng. Phys.*
- 538 Sensini, A., Gualandi, C., Cristofolini, L., Tozzi, G., Dicarolo, M., Teti, G., Mattioli-  
539 Belmonte, M., Focarete, M. L. (2017). Biofabrication of bundles of poly(lactic  
540 acid)-collagen blends mimicking the fascicles of the human Achille tendon.  
541 *Biofabrication*, **9**(1). <https://doi.org/10.1088/1758-5090/aa6204>
- 542 Sensini, A., Gualandi, C., Focarete, M. L., Belcari, J., Zucchelli, A., Boyle, L., Reilly,  
543 G. C., Kao, A. P., Tozzi, G., Cristofolini, L. (2019). Multiscale hierarchical  
544 bioresorbable scaffolds for the regeneration of tendons and ligaments.  
545 *Biofabrication*, **11**(3), 35026. <https://doi.org/10.1088/1758-5090/ab20ad>
- 546 Sensini, A., Gualandi, C., Zucchelli, A., Boyle, L., Kao, A. P., Reilly, G. C., Tozzi, G.,  
547 Cristofolini, L., Focarete, M. L. (2018). Tendon Fascicle-Inspired Nanofibrous  
548 Scaffold of Polylactic acid/Collagen with Enhanced 3D-Structure and  
549 Biomechanical Properties. *Sci. Rep.*, **8**(1), 1–15.  
550 <https://doi.org/https://doi.org/10.1038/s41598-018-35536-8>
- 551 Tseng, L. F., Mather, P. T., & Henderson, J. H. (2013). Shape-memory-actuated  
552 change in scaffold fiber alignment directs stem cell morphology. *Acta Biomater.*,  
553 **9**(11), 8790–8801. <https://doi.org/10.1016/j.actbio.2013.06.043>
- 554 Wu, S., Wang, Y., Streubel, P. N., & Duan, B. (2017). Living nanofiber yarn-based  
555 woven biotextiles for tendon tissue engineering using cell tri-culture and  
556 mechanical stimulation. *Acta Biomater.*, **62**, 102–115.  
557 <https://doi.org/10.1016/j.actbio.2017.08.043>
- 558 Xu, Y., Dong, S., Zhou, Q., Mo, X., Song, L., Hou, T., Wu J., Li, S., Li, Y., Li, P.,  
559 Gan, Y., Xu, J. (2014). The effect of mechanical stimulation on the maturation of  
560 TDSCs-poly(L-lactide-co-ε-caprolactone)/collagen scaffold constructs for tendon  
561 tissue engineering. *Biomaterials*, **35**(9), 2760–2772.  
562 <https://doi.org/10.1016/j.biomaterials.2013.12.042>
- 563 Youngstrom, D. W., & Barrett, J. G. (2016). Engineering tendon: Scaffolds,  
564 bioreactors, and models of regeneration. *Stem Cells Int.*, **2016**, 1–12.  
565 <https://doi.org/10.1155/2016/3919030>
- 566 Zidek, J., Vojtova, L., Abdel-Mohsen, A. M., Chmelik, J., Zikmund, T., Brtnikova, J.,  
567 Jakubicek, R., Zubal, L., Jan, J., Kaiser, J. (2016). Accurate micro-computed  
568 tomography imaging of pore spaces in collagen-based scaffold. *J. Mater. Sci.*

569  
570  
571

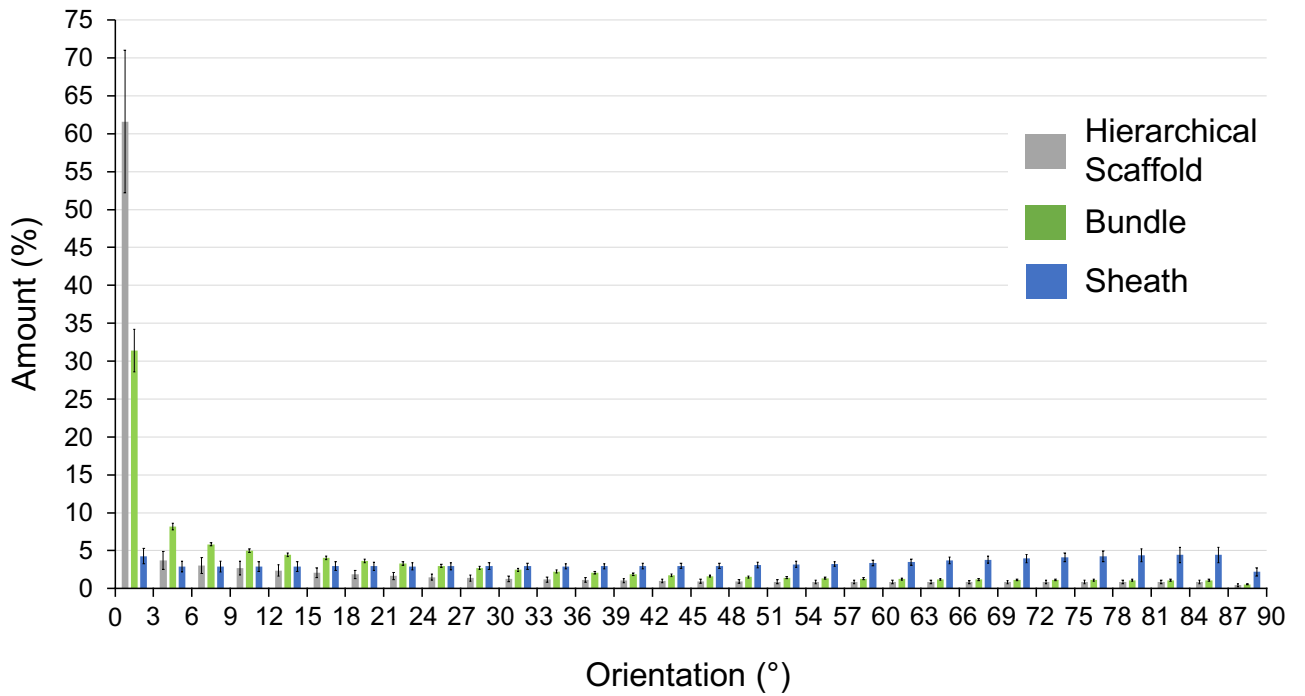
*Mater. Med.*, 27(6), 1–18. <https://doi.org/10.1007/s10856-016-5717-2>



572  
 573  
 574  
 575  
 576  
 577

**Fig. 1.** Workflow of the experiment. (A) Electrospun hierarchical scaffolds assembly (scale bar = 1 mm). (B) Fibroblasts culture: two scaffolds were cultured in static conditions, while other two with uniaxial sessions of stretching in a bioreactor. (C) Scaffolds preparation for the different imaging investigations (scale bar = 1 mm).





578

579

580

581

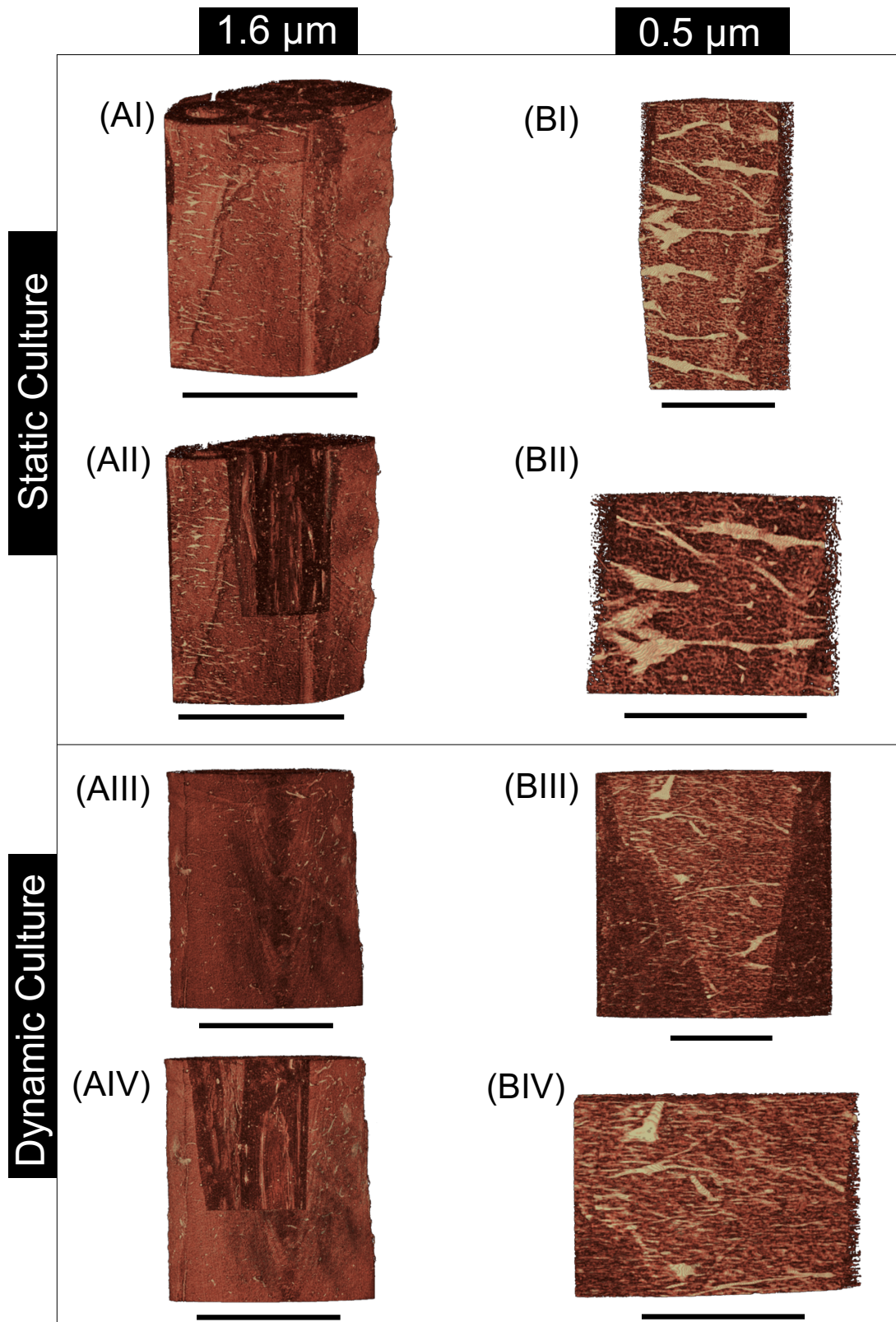
582

583

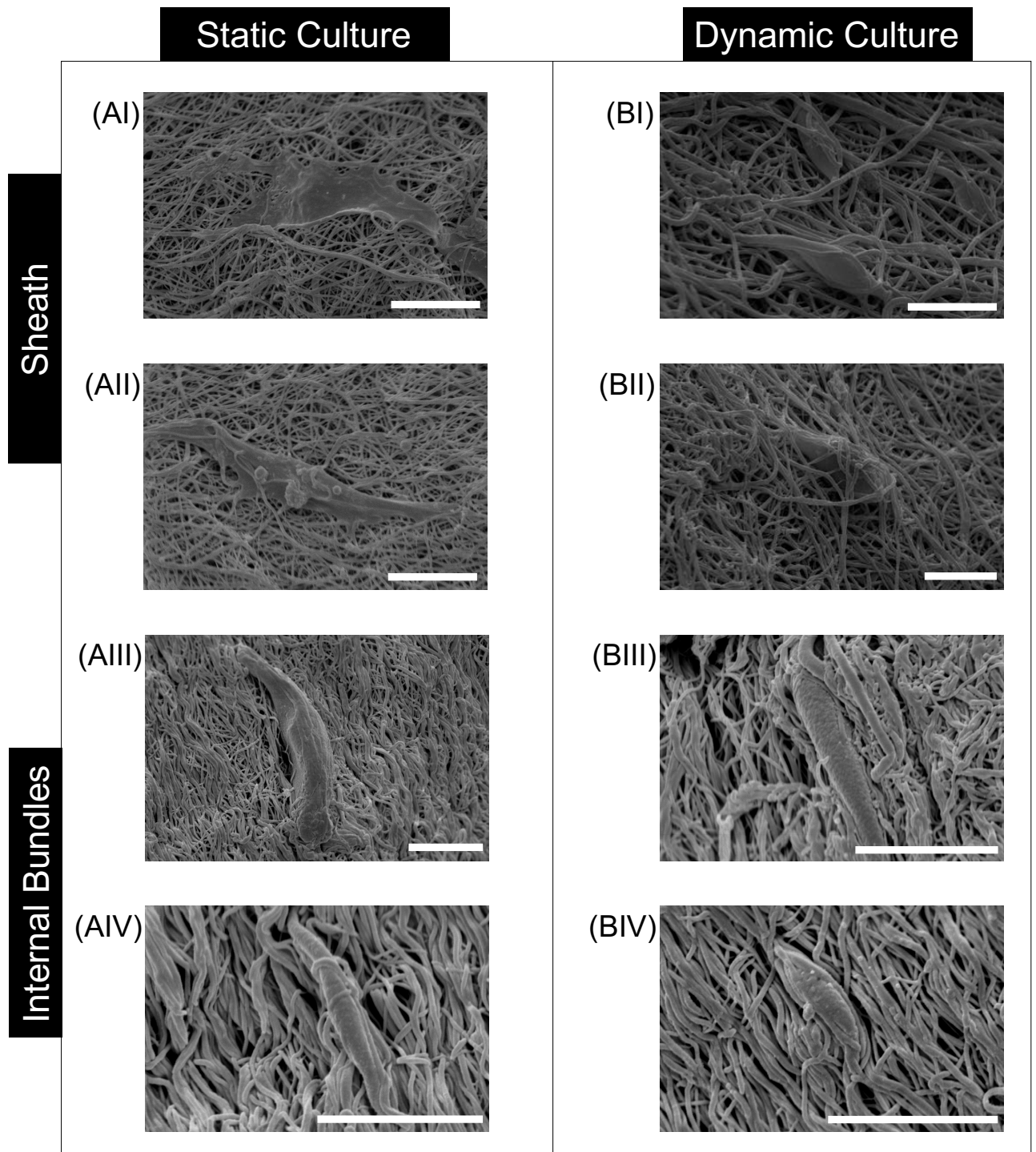
584

585

**Fig. 2.** Directionality analysis at different levels of the hierarchical scaffolds. The directionality histograms show the comparison between: the alignment of the bundles inside the hierarchical scaffold (gray bars), the distribution of nanofibers in the different directions for the bundle (green bars) and on the electrospun sheath (blue bars). An angle of 0° means that the nanofibers were aligned with the longitudinal axis of the hierarchical scaffold, an angle of 90° means that the nanofibers were perpendicular to it. Mean and standard deviation between images of the same specimen are plotted.

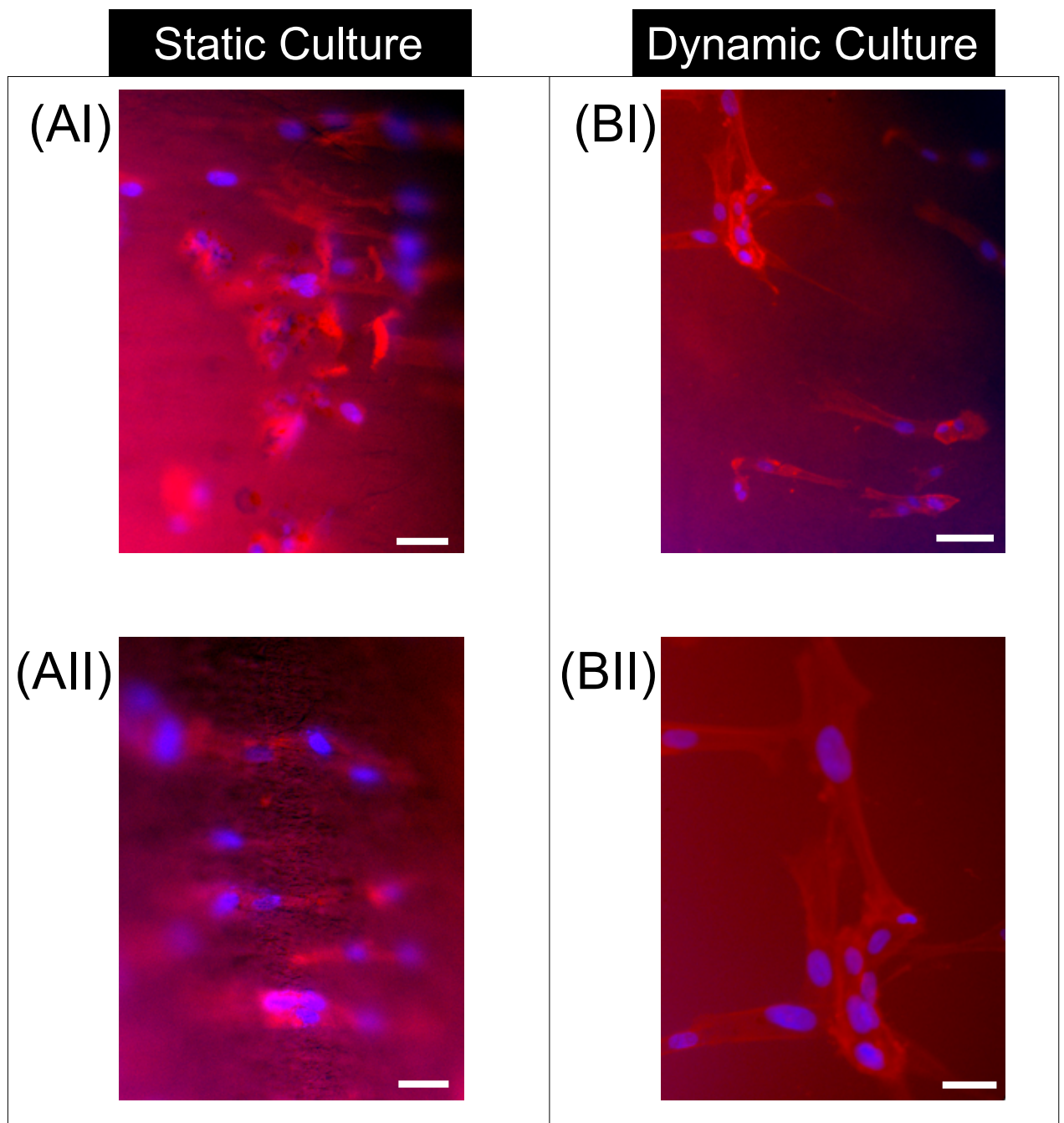


586  
 587 **Fig. 3.** XCT images of fibroblasts cultured onto the hierarchical scaffolds in static (I,  
 588 II) and dynamic (III, IV) conditions. (AI, III) Overview of the scaffolds; (AII, IV)  
 589 superficial crop showing the internal bundles (voxel size = 1.6 micrometers; scale bar  
 590 =1 mm). (BI, III) Overview of fibroblasts on the external sheath; (AII, IV) zoom on the  
 591 fibroblasts (voxel size = 0.5 micrometers; scale bar = 200 micrometers).



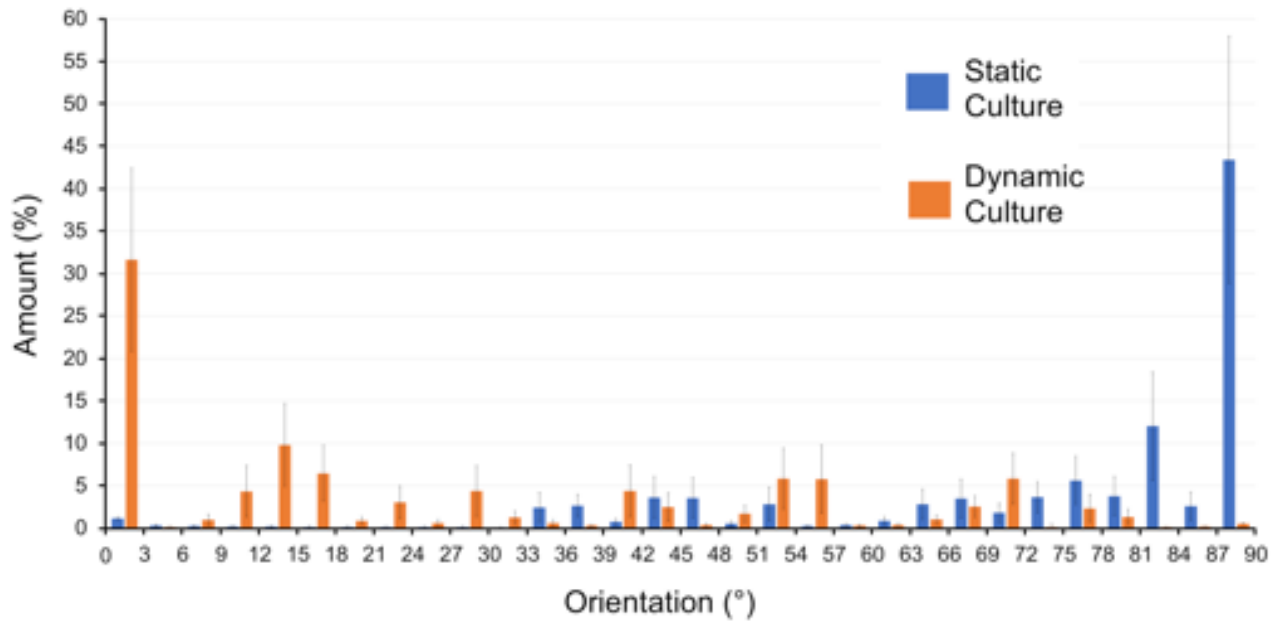
592  
593  
594  
595

**Fig. 4.** SEM images of fibroblasts cultured onto the hierarchical scaffolds in static (A) and dynamic (B) conditions (scale bar = 10 micrometers). (I-II) SEM images of the fibroblasts on the electrospun sheath; (III-IV) SEM fibroblasts on the internal bundles.



596  
597  
598

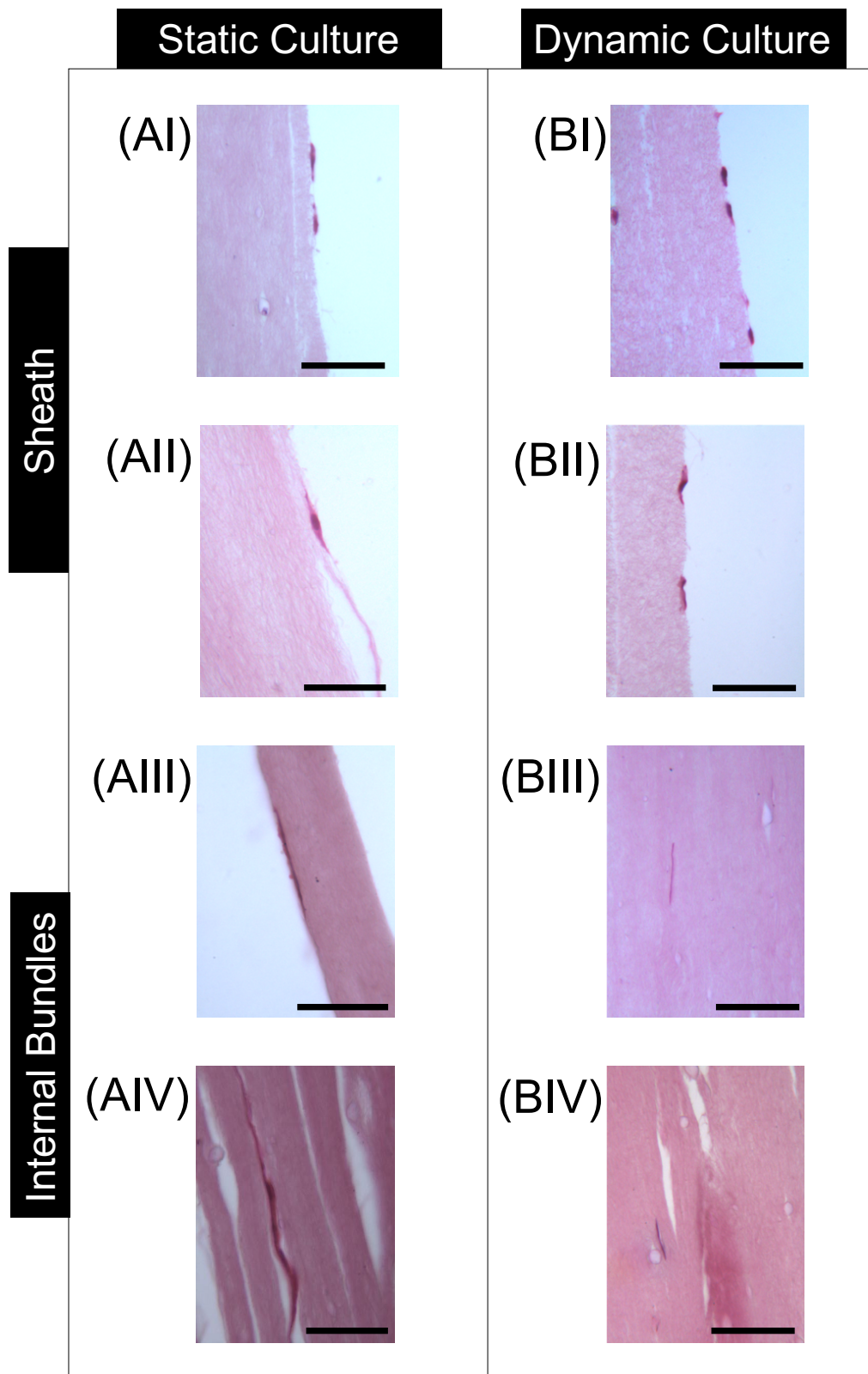
**Fig. 5.** Fluorescence images of fibroblasts onto the hierarchical scaffolds sheath in static (A) and dynamic (B) conditions (scale bar = 30 micrometers).



599  
 600  
 601  
 602  
 603  
 604  
 605

**Fig. 6.** Directionality analysis of cells grown on the electrospun sheaths (based on the orientation of the cells nuclei) in static and dynamic conditions of culture. An angle of 0° means that the cells were aligned with the longitudinal axis of the hierarchical scaffold, an angle of 90° means that the cells were perpendicular to it. Mean and standard deviation between images of the static and dynamic specimens are plotted.





606

607 **Fig. 7.** Histological investigation on the hierarchical scaffolds cultured in static (A) and  
 608 dynamic (B) conditions (scale bar = 50 micrometers). (I-II) Zoom-in on the fibroblasts  
 609 on the electrospun sheath; (III-IV) images of the elongated fibroblasts on the aligned  
 610 nanofibers of the internal bundles.

611